Micromechanical Modelling of Syntactic Foam

D. Carolan[a,b,*], A. Mayall[a], J. P. Dear[b], A. D. Fergusson[a,b]

[a] *FAC Technology, 53 Lydden Grove, London, SW18 4LW, UK*
[b] *Department of Mechanical Engineering, Imperial College London, London, SW7 2AZ, UK*

Abstract

A combined numerical-experimental method that enables accurate prediction of not only the elastic moduli and tensile failure strengths of syntactic foams, but also accounts for the experimentally observed scatter in these measurements is presented. In general, for the systems studied, an increase in microsphere content resulted in an increase in tensile modulus and a decrease in tensile strength. At low particle loading ratios, the variance in the measured experimental strength can be almost entirely attributed to the distribution of inter-particle distances between the microspheres, whilst at high particle loadings, geometric variance in the microstructure is shown to be only partially responsible for the observed scatter in strength data. Thus, for the first time, a direct link between the underlying microstructure and the experimentally observed scatter in fracture strength is drawn and substantiated with modelling.

Keywords: syntactic foam, numerical modelling, micromechanics

*Corresponding Author
Email address: declan@factechnology.com (D. Carolan)

1. Introduction

Composite foams are known as syntactic foams when filled with hollow microspheres. They are an efficient method to reduce weight in a high performance part without compromising on mechanical properties. This makes these materials particularly suitable candidates for applications in aerospace, marine, military and transport. In these applications, lightweight, load-bearing performance is crucial [1]. The porosity in a syntactic foam is located entirely within the impermeable shell of the microsphere [2]. Not only does this make these materials stronger and stiffer than conventional foams, it also limits moisture uptake, a key requirement for marine applications [3].

A micrograph of a densely packed syntactic foam is given in Figure 1. In this Figure, the microspheres are composed of borosilicate glass while the matrix is an epoxy resin. The foam can be seen to consist of three major phases, (1) the matrix, (2) the hollow glass spheres including both the external shell and the internal void and (3) some porosity external to the microspheres. The external porosity arises as a consequence of the manufacturing process where, due to the proximity of the microspheres to each other, the uncured resin has failed to completely fill the volume between the spheres. It can also be observed that the amount of matrix porosity is minimal, and so the effect of porosity is neglected in this work. By tailoring the individual structural and mechanical parameters of the syntactic foam composite such as the choice of matrix material, diameter and volume fraction of the microspheres, the optimum properties for a particular structural application can be achieved.

Experimental investigations are currently the most accurate and reliable

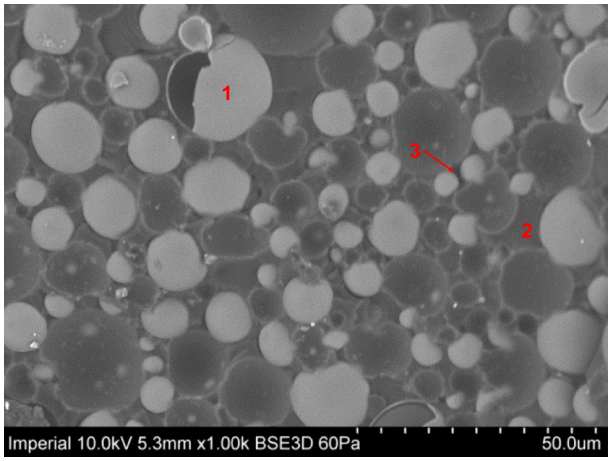

Figure 1: Scanning electron micrograph of a fractured syntactic foam sample. The volume fraction of the glass microspheres is $\approx 64\,\%$

method of obtaining mechanical properties of syntactic foams. Experimental investigations into the mechanical properties of syntactic foams have been conducted by several authors, including tensile properties [4–6], compressive properties [7–9] and flexural properties [10]. Analytical methods, adapted from those methods used to describe solid composite materials, have also been applied to syntactic foams although these have mainly focused on predicting the effective elastic properties of syntactic foams. As in the case of solid particulate composites, analytical models to predict the strength of a syntactic foam are almost non-existent in the literature.

Recently numerical methods, such as the Finite Element Method, have been used to model the syntactic foam using the smallest possible micromechanical unit cell structure, commonly referred to as the Representative Volume Element (RVE), to predict macroscopic material behaviour. Early modelling attempts by, for example, Marur [11] and Antunes *et al.* [12] focused

on determining the elastic properties of syntactic foams. These early studies adopted a unit cell approach and only briefly addressed the problem of particle-particle interactions. A summary of the efforts to use numerical approaches to homogenise the elastic properties of syntactic foams is provided by Bardella *et al.* [13] and other references therein.

Yu *et al.* [14] adopted a stochastic approach to the numerical prediction of the strength of syntactic foams. They used a random sequential adsorption approach to generate the microstructures. A condensing process proposed by Segurado and Llorca [15] was used to obtain a higher volume fraction of particles. Interactions between the glass microspheres and the matrix were assumed to obey a traction-separation law, although no physical justification for the choice of parameters was given by the authors. Nian *et al.* [16] reverted to a unit cell approach to model both the tensile modulus and strength of syntactic foams. Work by Bardella *et al.* [17] have modelled the failure of syntactic foam composites using a multi-particle unit cell approach. They use an average strain energy density to determine failure of the glass microspheres [18]. Bardella *et al.* actively model polydisperse systems by considering blends of different microspheres, although each microsphere within a family is considered to have a nominally identical radius. Moreover, they demonstrated that when microspheres are coated with polyurethane, this triggers a different failure mode than that observed for an untreated foam. A central open question left by the work of Bardella *et al.* is that their model predictions of failure only predict a very small variation with strength when considering a syntactic foam with either a low or high volume fraction of glass microspheres [18]. They duly note that their prediction

disagrees with experimental results reported by Gupta *et al.* [19]. Gupta *et al.* [19] and Tagliava *et al.* [20] both report a decrease in experimentally measured flexural strength as the volume fraction of microspheres increases.

Many of these earlier works have emphasised the brittle nature of the failure of syntactic foams. Indeed, a thorough inspection of the experimental results show significant error bars on the reported strength values. Brittle failure typically implies a natural degree of scatter in the strength of nominally identical specimens. Understanding the source of scatter has important engineering and design implications. The strength that can be safely used for design will be less than the average strength. The allowable design strength will depend on the exact form of the distribution of strengths measured experimentally. The current work aims to build on the recent literature and make numerical predictions of the observed experimental variance in the fracture strength.

2. Computational Model

2.1. Generation of Model Geometry

A common method used to study the micromechanics of particulate composites is to assume that the bulk strength behaviour of the particles can be adequately described by a regular arrangement of particles e.g. [21–23]. The assumption of regularity, while providing detailed information on the interaction between particles, does not account for the variation in inter-particle distance that would be commonly encountered in a real micro- or nano-composite. These models are therefore unable to predict experimentally observed variations in the strength of syntactic foams, which often fail

in a brittle manner and with a high degree of scatter associated with the measured failure strength [24].

The random sequential algorithm (RSA) [25] is widely applied to generate random distribution of microspheres within a unit cell. In the first step in the algorithm, the position of the first particle is randomly selected within the unit cell. Next, the position of the second particle is selected and a collision check is performed between the two particles. If an overlap is detected, then the positioning of the second particle is replaced until no overlap is detected. This process is repeated with each new particle being checked for collisions with all of the previously placed particles. While this algorithm is elegant in its simplicity, it is not efficient to use for high volume fractions of particles. Indeed, several authors have reported only achieving volume fractions of up to 30% in three-dimensional space using this method [15, 24, 26].

In order to obtain packing fractions approaching the random close packing limit of 64%, the approach first outlined by Lubachevsky and Stillinger [27] for close packing of disks is adopted. A variation of this algorithm was used by Bardella *et al.* [17]. This algorithm is based on a molecular dynamics approach where the particles move around inside a volume an interact with each other. In the first instance, the desired number of particles are placed within the unit cell using the RSA approach described previously. The individual particles are sized such that they occupy a very small volume in comparison to the overall volume of the space which is to be packed. A velocity vector, v_i is assigned to each particle and each particle is prescribed a growth rate with respect to time. The first time-step, dt, is calculated to coincide with the time of the first particle-particle collision, i.e. event driven

simulation. Subsequent time-steps are calculated using the same approach. The radius of the particles, r_i, at each time-step, i, increase according to the following growth law:

$$r_i = r_{0,i}(1 + kt) \tag{1}$$

where $r_{0,i}$ is the initial radius of the i^{th} particle and k is a small positive value chosen to control the rate of growth. The choice of k is not arbitrary but can greatly affect the packing dynamics of the system. In general a large value relative to the particle velocities will cause a jammed irregular configuration while very small values will result in a much more crystalline packing. Indeed, Lubachevsky and Stillinger have surmised that in the limit $a+ \rightarrow 0$ the algorithm should eventually reach the maximum packing fraction allowable. Collisions between particles are treated elastically. The treatment of particles which intersect the boundary of the unit cell have been dealt with in two ways. The first option that has been implemented within the procedure limits particles to be contained entirely within the unit cell; i.e. there are no particles intersecting the boundary, a 'hard' boundary condition whereby any particles which intersect the boundary reflect of the cell wall. Such a system is preferable because non-physical stress concentrations occurring at the interface between the microspheres, matrix and the boundary of the representative volume failure, which can cause premature failure of the model, are produced. The procedure is also capable of handling particles which intersect the surface of the RVE by prescribing periodic boundary conditions on the faces of the unit cell. This means that when a particle or part of a particle leaves the unit cell through a face, it reappears at the opposing face. This represents a so-called 'soft' boundary condition and results in models

which can be used to accurately explore the maximum packing fraction of different families of particles. A flowchart outlining the main steps and sequencing involve in the particle the particle placement algorithm is given in Figure **??**.

2.2. Construction of the Finite Element Model

A Python script was used to automate the pre- and post-processing of the finite element models in Abaqus 6.12 [28]. An example of typical microstructures generated with a 'soft' boundary condition is given in Figure 3. The positions and radii of the spherical particles generated via the Lubachevsky-Stillinger algorithm described in Section 2.1 are used as inputs for generation of the model. The automated nature of the finite element implementation allows the simultaneous investigation of many instantiations of randomly generated models at a specified volume fraction with minimal user interaction. This allows the examination of statistical variation in measured properties at a specified volume of microspheres. The stochastic models were meshed automatically using 4-node tetrahedral element for the matrix (C3D4), 8-node cohesive elements for the microsphere/matrix interface, COH3D8, and 8-node hexahedral elements for the microspheres (C3D8R). The model uses the mm-MPa system of units with the global mesh size set at $0.5r_{ms}$, where r_{ms} is the microsphere radius. A mesh convergence study was conducted to ensure that at the chosen mesh size, the results were independent of the meshing approach. The mesh size was automatically refined locally for the microspheres, at the microsphere/matrix interface and for the cohesive elements. In order to avoid meshing errors when running the model, two checks were defined within the pre-processing step. The first defines a minimum

distance that a sphere must be from any boundary in the unit cell, this was set as $0.1r_{ms}$. If the sphere is within the unit cell then it is included in the model. The second check ensures that the spheres are not touching. Finally, the microspheres are scaled such that there is at least a distance of $0.1r_{ms}$ between microspheres. This allows the insertion of a thin layer of cohesive elements around each microsphere. The cohesive elements govern the debonding behaviour of the microspheres from the matrix.

Each representative volume element was subjected to a steadily increasing quasi-static strain in the positive x-direction. Brittle failure was prescribed in both the glass microspheres and the matrix resin. Symmetry planes were applied to the faces of the model pointing in the negative x, y and z direction respectively, while the remaining faces were set as traction-free. The simulations were run using Abaqus/Explicit. This allows the numerical framework to effectively model the the complete fracture process, whereas an implicit procedure would fail to converge once the strong non-linearities associated with cracking begin to appear. As no strain rate effects are expected at quasi-static rates of loading, mass scaling was used to reduce the runtime of the models while ensuring that inertial effects remained negligible.

The model was split into two steps, each with a defined number of output time intervals, in order to reduce the computational time for each model. The first step comprises of 5 time intervals up to 20% of the applied strain. From 20% to 100% of applied load 60 time intervals were prescribed. The Python script also automatically generates the stress-strain curve for each simulation. Only eight time intervals were used for post processing purposes - the initial four time-steps were used to evaluate the tensile modulus, while the final

Table 1: Material properties used in the current work.

Properties	Matrix	Microspheres
Young's modulus [GPa]	3.17	70
Poisson's ratio [-]	0.35	0.2
Failure strength [MPa]	93.25	965
Fracture energy [J/m^2]	100	6 [30]

four intervals prior to failure were used to evaluate the failure strength. The strain was taken as the applied strain at the time interval of the simulation, whilst the stress was calculated using the volumetric homogenisation method [29].

2.3. Material properties

The material properties are shown in Table 1. The epoxy matrix is modelled as a linear elastic material and the microsphere particles are the IM30K hollow glass microspheres from 3M, with an average diameter of $16\mu m$, and a particle radius to wall thickness fraction of 10 [31]. In the current work no consideration was given to the distribution of particle size of the IM30K glass microspheres. Both materials were assumed to behave in a brittle manner. The failure strength of the glass microspheres was estimated based on the reported crush strength, 193 MPa, as per the data sheet. The reported crush strength is the pressure at which 90% of the microspheres have survived a hydrostatic compression test. Treating the microspheres as a thin walled spherical vessel, it can be noted that the maximum stress in the microsphere

wall can then be calculated by:

$$\sigma = \frac{PR_{ms}}{2t_w}, \tag{2}$$

where P is the applied pressure and R_{ms}/t_w is the ratio of the particle radius to wall thickness. Thus, the estimated failure strength of the glass microspheres is calculated as $5P = 5 \times 193 = 965$ MPa. It is important to note that this value is a compressive strength being used as a tensile failure stress in the numerical models. This can be rationalised by considering the extremely small value of the wall thickness, i.e. sub-micron, and noting the reduced potential for the existence of a flaw exceeding the critical flaw size at this length scale. It is therefore not unreasonable, in the absence of better information, to then assume that the tensile and compressive strengths of the glass are equal at this length scale.

The fracture energy of the glass was taken from the literature as 6 J/m^2[30]. The fracture energy of the epoxy matrix was measured directly using single-edge notch bend tests. The second parameter required to construct the cohesive zone model, the fracture strength, is difficult to measure independently but is expected to be of the order of the tensile yield strength. The fracture strength and fracture energy of the cohesive interface between the microspheres and the matrix are also unknown. However, a close examination of the fracture surface in Figure 1 reveals glass microspheres with a very clean and smooth surface, with little evidence of residual epoxy adhering to the surface of the particles. This indicates that the values for interface cohesive strength and fracture energy should be significantly lower than that of the resin matrix.

Finally, it is important to note the limitations of the models, when com-

pared to real world materials and applications. We have assumed that all of the microspheres have the same diameter, i.e. the nominal diameter given by the datasheet [31]. Incorporating polydispersity into the model can be readily achieved, but the size of the micromechanical model required to be statistically representative can become unduly large. Bardella *et al.* [18] have presented work on polydisperse spheres and demonstrate the ability to predict the order of collapse of the microspheres under compression, namely the lightest microspheres collapse first. In the current work the high-strength microspheres are never observed to collapse. Thus, the role of polydispersity is relatively unimportant for the syntactic foam presented here. However, in order to extend the functionality and applicability of the models presented here to model syntactic foams manufactured with low strength microspheres, or blends of high and low strength microspheres, the role of polydispersity would have to be considered. For similar reasons, the effect of the presence of matrix voids have also been neglected. Matrix voids do exist and are especially prevalent at high volume fraction syntactic foams. Nevertheless, in spite of the idealisations and simplifications made in the model, some important information can be obtained about the behaviour of syntactic foam composites.

3. Experimental Methods

3.1. Materials

A standard diglycidylether of bis-phenol A (DGEBA) epoxy resin was used as the base resin in the current work. The resin, Araldite LY556, was obtained from Huntsman, UK and has an epoxide equivalent weight (EEW)

of 185 g/eq. The curing agent used was iso-phorone diamine (IPD) obtained from Sigma=Aldrich, UK, with an amine equivalent weight of 43 g/eq. Samples containing 10-30% microsphere volume fractions were manufactured by combining the resin and curing agent in the stoichiometric ratio. The required amount of microspheres, with the appearance of a fine powder, were then added to the mixture under continuous stirring to ensure the microspheres were adequately dispersed. The mixture was subsequently degassed in a vacuum chamber for 10 minutes and a plaque of material cast in a silicone mould. Samples of 40 and 50% microsphere volume fraction could not be made using this method as the sheer quantity of microspheres in the resin forms a highly viscous paste. This resulted in an inhomogeneous mixture of microsphere dense and resin dense regions which are unsuitable for testing. The highest volume fraction sample, nominally 60% volume fraction, was manufactured using a closed mould under pressure. This method overcomes the problem of microsphere agglomeration but does not allow precise control of the volume fraction in the resultant composite; and only tightly packed samples can be made, i.e. systems with a particle volume fraction close to their maximum theoretical volume fraction of randomly packed particles.

3.2. Determination of tensile properties

Tensile tests were performed on the bulk epoxy resin as well as the glass microsphere modified epoxy systems to obtain the tensile Young's modulus and the tensile failure strength. The tests were conducted in accordance with ISO-527 [32]. Dumbbell shaped specimens of type 5A with a gauge length of 30 mm were machined from 3 mm thick cast plaques of material. The tests were conducted at a constant crosshead displacement rate of 1 mm/min with

the strain measured directly on the sample using a clip-gauge extensometer. Each tensile test sample was carefully prepared by polishing the edges of the sample within the gauge length to ensure a smooth finish and to minimise the influence of the sample preparation on the fracture strength. At least five specimens were tested for each formulation in order to assess the variability of Young's modulus. An additional 15 specimens were tested in order to generate enough experimental data to statistically analyse the variation in fracture strength of the glass-microsphere modified epoxy composites.

4. Results and Discussion

4.1. Experimental Results

The experimentally determined values of Young's modulus and fracture strength are given in Table 2. It can be seen that the Young's modulus increases with the addition of glass microspheres up to 40 vol.%. No further increase was observed with increased microsphere loading of ≈60 vol.%. The fracture strength was observed to decrease with increasing particle loading. It is of interest to note that the standard deviation of the fracture strengths also decreases with increased particle loading, excluding the results for the resin without any particulate modification. This will be discussed further in conjunction with the numerical predictions.

Analytical models for predicting the strength of particulate composites are less prevalent in the literature than those for predicting the moduli. A common approach assumes that the strength is determined by the effective area of load-bearing matrix. This gives rise to equations where the strength

Table 2: Experimentally measured mechanical properties of different syntactic foam formulations.

v_f	E [GPa]	σ_f [MPa]
0	2.90±0.09	76.3±4.8
10	2.96±0.27	64.9±10.2
20	3.62±0.18	55.4±10.0
30	3.99±0.27	43.3±7.1
40	4.88±0.33	-
60	4.79±0.30	34.9±2.8

is described by a power law.

$$\sigma_c = \sigma_m(1 - aV_p^n) \tag{3}$$

where σ_c and σ_m are the strengths of the composite and matrix respectively, V_p is the volume fraction of the reinforcing particle and a and n are constants that depend on the particle geometry and arrangement in the composite. Nielsen [33] introduced the concept of a stress-concentration factor and, for particles arranged cubically in a matrix, arrived at the following relationship

$$\sigma_c = \sigma_m(1 - V_p^{2/3})K \tag{4}$$

where K is the stress concentration factor. Nielsen suggested that a suitable value of K as 0.5. Nicolais and Narkis [34] also considered a matrix with particles arranged in a cubic format. They assumed that fracture took place in the minimum cross-section of the matrix phase. Equation 3 can then be rewritten as:

$$\sigma_c = \sigma_m(1 - 1.21V_p^{2/3}) \tag{5}$$

The experimentally obtained fracture strengths are plotted in Figure 4. Predictions made using both the Nielsen model and the Nicolais-Narkis model are also given. In each of these models, the fracture strength of the unmodified epoxy was used as the matrix strength, i.e. $\sigma_m = 76.3$ MPa. Using a stress concentration factor of, $K = 0.5$, as suggested by Nielsen results in very poor agreement between the experimental observations and the analytical predictions. A value of $K = 1$ gives a much better agreement with the experimental observations, although there is still significant under-prediction of the fracture strength for syntactic foams with a very high volume fractions of particles. The Nicolais-Narkis model under-predicts the experimental observations and is in general a poorer indicator of the experimental than the Nielsen model, $K = 1$. Finally, it is important to observe that both of the analytical models employed are unable to capture the large standard deviations in the experimental data, but only provide an average value of fracture strength.

4.2. Numerical Predictions

4.2.1. Calibration of the cohesive properties

The failure parameters of the cohesive law, fracture energy and cohesive strength, can be difficult to extract experimentally. Previous methods have relied on calibration with experimental data. While the equivalent resin failure properties can be derived from macroscopic experiments, e.g. fracture toughness tests, differences in stress states at the microscopic level mean they may not be the correct properties to use at the microstructural scale. As such a calibration process was conducted. This calibration process follows a similar approach to that outlined by Carolan et al. [35]. The first assump-

tion in the process is that fracture strength in tension is likely to be strongly dependent on the cohesive strength damage parameters and more weakly dependent on the cohesive fracture energy. The process relies on recognising that when adjusting either of the cohesive strength damage parameters, i.e. σ_m or σ_{int}, the effect of adjusting either parameter independently of the other on the predicted failure strength of the syntactic foam will be pronounced to a greater or lesser degree in the materials with a high volume fraction of microspheres than those with a low volume fraction of microspheres. Similarly, adjusting the fracture energy of either the interface, G_{int}, or of the matrix, G_m will affect the predicted macroscopic fracture strength to a greater or lesser degree, depending on the microsphere volume fraction. Since, these parameters are assumed to be a constant, i.e. it is assumed that the cohesive properties of the resin, σ_m and G_m, and of the interface, σ_{int} and G_{int}, do not change with microsphere volume fraction, it is possible to isolate a particular combination of these four parameters that best predict the experimental behaviour of the syntactic foams over the range of entire volume fractions investigated.

The calibration process begins with an initial estimate for the cohesive properties of the matrix and the interface, σ_m, G_m, σ_{int} and G_{int}. For the matrix properties, it is prudent to take the experimentally measured values outlined in Section 4.1. The interface properties are much more difficult to measure, but some logical assumptions can be made to make a good first approximation of the relevant values. First, it can be assumed that the properties will be of the order of the cohesive properties of the matrix. Moreover, the fracture surface presented in Figure 1 clearly show clean microspheres with

no residual resin on the particles. This implies that the adhesion between the microspheres and the resin is relatively poor, so it would be expected that $\sigma_{int} < \sigma_m$ and $G_{int} < G_m$.

Sensible upper and lower bounds on the cohesive properties of the interface and matrix are selected. The initial upper bounds for both the resin and interface are set to be twice the values measured experimentally, while the initial lower bound is set to some arbitrarily small value. The initial values for the optimisation routine are chosen according to the following rules.

$$G(i) = \frac{G_{lb} + G_{ub}}{2} \tag{6}$$

$$\sigma(i) = \frac{\sigma_{lb} + \sigma_{ub}}{2} \tag{7}$$

where i represents the iteration number and lb and ub denote the lower and upper bound respectively. A reduced number ($n = 5$) of models are evaluated at each volume fraction and the mean failure strength from the models, σ_{num}, is compared to the mean failure strength from the experimental data, σ_{exp}. The upper and lower bounds for the cohesive properties are then updated according to the rules outlined in Table 3. In order to speed up the calibration process, the unit cell with the failure strength closest to the mean value is automatically selected and only this unit cell is evaluated over the remaining iterations. The optimisation routine is terminated once the cohesive properties change by less than 1% between iterations. The calibration procedure for the cohesive properties of the interface and resin are run sequentially. Following the calibration procedure the cohesive properties used in the numerical model for the interface and resin are chosen as. $G_{int} = 0.04$ kJ/m^2, $G_{res} = 0.075$ kJ/m^2, $\sigma_{int} = 23.2$ MPa and $\sigma_{resin} = 102.8$ MPa. The value

of interfacial strength arrived at as a result of the calibration process agrees well with values reported previously in the literature for syntactic foams [6] and glass fibre epoxy composites [36–38].

It is of interest to note that the calibration procedure has changed the values of cohesive strength and fracture energy from those measured in the bulk resin via fracture testing. The fracture energy has decreased from 0.100 kJ/m^2 to 0.075 kJ/m^2 while the cohesive strength has increased marginally from 93.25 MPa to 102.8 MPa. While the exact reason for this change has not been investigated, it is thought to be related to the effect the particles have on locally increasing the level of constraint in the matrix, forcing the epoxy matrix to behave as a stronger, more brittle material.

Table 3: Optimisation rules for updating cohesive properties.

Case	10 vol. %	55 vol. %
$\sigma_{num} < \sigma_{exp}$	$G_{lb}(i+1) = \frac{G(i)+G_{lb}(i)}{2}$	$\sigma_{lb}(i+1) = \frac{\sigma(i)+\sigma_{lb}(i)}{2}$
$\sigma_{num} > \sigma_{exp}$	$G_{ub}(i+1) = \frac{G(i)+G_{ub}(i)}{2}$	$\sigma_{ub}(i+1) = \frac{\sigma(i)+\sigma_{ub}(i)}{2}$

4.2.2. Tensile Modulus

The numerically predicted tensile modulus is plotted in Figure 5 and compared to the experimentally obtained results. Reasonably good agreement between the numerical predictions and the experimentally measured values is observed. The micromechanical numerical model is capable of picking up the plateau in Young's modulus observed experimentally, although the numerical model does under predict the Young's modulus of highly filled syntactic foams.

4.2.3. Failure strength

Figure 6 presents a comparison of the numerical predictions of failure strength made by the micromechanical method developed in this work with the experimentally observed failure strengths. Excellent agreement is observed between the predictions and measurements indicating that the developed model is capable of predicting the tensile failure response of polymer-matrix glass-microsphere syntactic foams across a wide range of particle loadings. This result is, in and of itself, hardly surprising, since the general trend of decreasing strength with increasing particle loading can be recovered by the simple analytical models such as Nicolais-Narkis and Nielsen and the cohesive parameters used in the study were calibrated using representative microstructural geometries from the study. The numerical model however, does reveal some interesting information when considering the experimentally observed scatter in failure strengths. The standard deviation of both the experimentally measured and numerically predicted failure strength, $SD(\sigma_f)$, is plotted in Figure 7. It can be observed that, both in the experiment and in the numerical model, the standard deviation of the strength decreases with increasing microsphere loading. A similar reduction in standard deviation with increased microsphere loading was reported by Tagliava et al. [20] for flexural strength results, although no remark on the significance of this result. However, Gupta *et al.* reported no obvious trend in standard deviation for compressive strength. Both Tagliava *et al.* and Gupta *et al.* investigated the same vinyl ester, glass syntactic foam composites. Moreover, in the current work, there is remarkable agreement in the degree of scatter obtained between the experimental measurements and the numerical predictions. This

lends the presented numerical model a predictive power not reported before in the literature; an ability to describe the scatter observed in strength experiments.

In the current work, the only difference between different instantiations of a microstructural model at a given volume fraction is the geometry, i.e. the positions of the microspheres within the unit cell relative to each other. All other possible variables have been kept constant, e.g. σ_{int}, although in reality, these values may differ from microsphere to microsphere, and even across the surface of one microsphere. Thus, it is apparent that the experimentally obtained variation in fracture strength, σ_f, can, at least in part, be attributable to the randomness of the underlying microstructure. To emphasise this point, the variation in the distribution of microspheres was measured at each volume fraction. For each microsphere, the nearest neighbour, ie. the microsphere closest to that microsphere, was identified. The distance between the pair of nearest neighbour microspheres was subsequently computed. This is termed the inter-particle distance, (IPD). Finally, the standard deviation of these computed distances was then taken as a single-value representation of the randomness of the microsphere placements. In Figure 8 the standard deviation of the numerically obtained fracture strength, SD(σ_f), is plotted versus the standard deviation of the inter-particle distance, d_{IPD}, normalised with respect to the diameter of the microspheres, d_{ms}. A very strong correlation between the variation in microstructural geometry and the variation in syntactic foam strength can be observed. The evidence presented in Figure 8 strongly supports the argument that variation in fracture strength of syntactic foams is governed by the microstructure.

4.3. Weibull Analysis

Strength measurements of nominally identical syntactic foam specimens typically exhibit large degrees of scatter in the measured data [39]. Consequently, the strength of syntactic foams is poorly defined using an approach based solely on considering the average and standard deviation of the experimentally measured strengths. A more informative approach is to use Weibull statistics to quantitatively characterise the scatter in strength data.

The Weibull distribution has been used extensively in the ceramics community to accurately describe the strength distribution of brittle materials [40–43]. This theory assumes a direct correlation between the density of flaws, and the subsequent strength distribution. In the micromechanical models, the flaws can be assumed to be the glass microspheres. The theory is based on the weakest link hypothesis, whereby specimen failure is due to the failure of the weakest volume element. While recent research may have shown this not to be strictly accurate, the distribution does provide a simple and straightforward characterisation method [42, 43]. For a three-parameter Weibull distribution the cumulative failure probability of a material subjected to a uniform stress, σ is given by:

$$F(\sigma) = 1 - e^{\left(-\left[\frac{\sigma-\sigma_{th}}{\sigma_0}\right]^m\right)} \tag{8}$$

where σ_0 is the characteristic Weibull strength, σ_{th} is a threshold strength, below which no failure will occur, and m is the shape parameter for the Weibull distribution, known as the Weibull modulus. A low Weibull modulus, m, is indicative of a wide degree of scatter in the measured strength data. For most brittle materials, this is of the order of 1-10 [44]. Equation 8 is a

three-parameter distribution. For many materials the threshold strength, σ_{th} is taken to be zero and the distribution reduces to the more commonly used two-parameter distribution. Wachtman et al. [44] have described a second type of three parameter distribution, whose cumulative failure probability is described by:

$$F_P(\sigma) = 1 - e^{\left(-\left[\frac{\sigma}{\sigma_0}\right]^m + \left[\frac{\sigma_P}{\sigma_0}\right]^m\right)} \tag{9}$$

where σ_P is the proof stress. Note that Equation 9 is not equivalent to the classic three-parameter distribution in Equation 8. Wachtman proposes it as an alternative three parameter distribution which has found considerable application in describing the variation in strength data after a proof stress procedure has been carried out. This form of the distribution better represents the data in the current work.

Figure 9 presents a statistical comparison between the experimental measurements and the numerical predictions for syntactic foam composites at low volume fraction, 10%, and at high volume fraction, 55%-60%. A number of observations may be made from a close inspection of these graphs. Firstly, there is excellent agreement between the experimental measurements and the numerical predictions for the stochastic models with a microsphere volume fraction of 10%. Both the experimental results and the numerical predictions exhibit a lower tail to the distributions. As discussed previously, the existence of a lower tail to the distribution indicates some lower bound, or proof stress, below which failure will not occur. One can also argue about the existence of an upper bound in the experimental and numerical data presented for the 10 vol.% syntactic foams. In a similar argument to that made for the lower tail, the existence of an upper tail indicates that there also exists

anmaximum strength which can be achieved in the syntactic foam composite. The excellent agreement between experiment and prediction implies that the variation in the underlying microstructure is indeed responsible for the observed variation in fracture strengths experimentally.

In the case of the highly filled syntactic foam, the correlation between the experimental measurements and numerical predictions is not as good as in the case at lower volume fractions. The stochastic models predicted a slightly tighter distribution than the experimental observations. Nevertheless, the essential features of the three-parameter Weibull distribution are still captured, i.e. the existence of a lower tail to the Weibull distribution. In a highly filled syntactic foam composite, where the particle volume fraction approaches the random close packing limit, there cannot be much variation in microstructure, in terms of the distance between particles. Any variation between microstructures can only manifest as a variation in the inclination of the vector connecting nearest neighbour centres to the direction of the applied external loading. Indeed, at the random close packing limit, all microspheres (except rattlers that occur sporadically), will be touching their nearest neighbours by definition. Thus the geometric variation in the the microstructure alone, is insufficient to explain the observed variance in fracture strength.

4.4. Parametric Study

To further understand the role of the matrix, σ_{resin} and interface, σ_{int} strength on the failure behaviour of syntactic foam composites a parametric study was carried out. For each volume fraction, the matrix strength, σ_{resin}, was increased and decreased by 50%, i.e. $1.5 \times \sigma_{resin}$ and $0.67 \times \sigma_{resin}$, while

keeping the value of the interface strength, σ_{int} constant. The results of this study are presented in Figure 10 (a). It can be seen that by changing the value of σ_{resin}, large differences in the average fracture strength can be obtained at low volume fractions of microspheres, while for heavily loaded syntactic foam composites, no significant changes can be observed,

Figure 10 (b) presents the results of the corollary, whereby the interface strength, σ_{int} was increased and decreased by 50% with σ_{resin} held constant. While some differences in average fracture strength can be observed at low volume fractions, these are not as significant as in the case presented in Figure 10 (a). Moreover, large improvements in the average fracture strength can be made for highly filled composite syntactic foams by adjusting the interface strength.

Once again, the use of Weibull statistics to analyse the stochastic models provides much more insight into the underlying behaviour. The effect of varying the cohesive strength of the resin, σ_{resin}, on the resulting Weibull distribution of fracture strengths is given in Figure 11 for a volume fraction of (a) 10% and (c) 55-60%, while the effect of varying the cohesive strength of the interface, σ_{int}, is given in Figure 11 (b) and (d) for the same volume fractions. The vertical lines represent the input cohesive strength values of either the resin or the interface.

In the case of a low volume fraction syntactic foam composite, increasing or decreasing σ_{resin} by 50%, Figure 11, does not alter the shape of the Weibull distribution, except that the entire curve shifts to higher values of strength, this means that the Weibull modulus, m, does not change significantly, but the characteristic strength, σ_0 does. On the other hand, modulating the

value of σ_{int}, Figure 11 (b), does not have much of an effect on the fracture strengths recorded at the upper end of the distribution, but a divergence in fracture strengths is noted at progressively lower strength values. Indeed, in the case where σ_{int} is reduced to $0.67\times\sigma_{int}$ a very significant lower tail emerges. The scatter in the experimental values increase and a reduction in the Weibull modulus is thus calculated.

A different picture appears when one considers the high volume fraction syntactic foams. Adjusting the cohesive strength of the resin, σ_{resin}, as shown in Figure 11 (c) has very little effect on the distribution at the lower end of the predicted values, but a divergence at the upper end is predicted. While a potential increase in the characteristic strength of the syntactic foam is obviously welcome, in this case, it is tempered by a reduction in Weibull modulus. Finally, adjusting the cohesive interface strength, σ_{int}, has the effect of translating the predicted fracture strengths, much like the effect adjusting σ_{resin} had in Figure 11 (a).

Thus, it appears that the tensile fracture behaviour of syntactic foams is governed by the strength properties of the matrix when low volume fraction syntactic foams are considered, but by the interfacial strength between the microspheres and the matrix when high volume fractions are concerned. Moreover, the extreme upper and lower values of fracture strength predicted using the micromechanical models are conservatively bounded by the cohesive properties of the interface and the resin. From a design point of view, it would be preferable to design using predictable material properties. Such a material would have as high Weibull modulus, m, i.e. a low scatter in strength properties. The numerical models suggest that such an increase in

m can be achieved by reducing the gap between the cohesive strength of the matrix, σ_{resin}, and that of the interface between the microspheres and the matrix, σ_{int}.

5. Conclusions

A numerical method for predicting the mechanical properties of syntactic foams has been developed. The method is capable of predicting the failure of syntactic foams across a wide range of particle loading, from very low volume fraction up to systems where the particle packing fraction approaches the random close packing limit. The importance of the correct choice of both numerical homogenisation scheme and initial cohesive stiffness when formulating a micromechanical model is demonstrated. Moreover, the model can predict the expected variance in fracture strength for a given microsphere volume fraction. The variation in fracture strength has been linked to the randomness of the underlying geometry. A sensitivity study of the cohesive parameters controlling the failure mechanisms has demonstrated that, at high microsphere volume fraction, the strength of the cohesive interface is critical in controlling the overall failure strength of the syntactic foam, while at low microsphere volume fractions, the strength of the matrix is more important. The results highlight the importance of considering randomness and variation in the microstructure of syntactic foam composites, or indeed particulate composites in general. The modelling approach developed has allowed, for the first time, accurate predictions of the mechanical performance including the experimentally observed scatter of this important class of materials. These materials are finding novel application in the aerospace, marine

and transport sectors. The combined experiments and modelling presented can be used to design stronger syntactic foam composites and allow for more robust design of components containing syntactic foam composites

6. Acknowledgements

D. Carolan would like to acknowledge the financial support of *Marie Curie Actions* under the *Society & Enterprise* Fellowship scheme. The financial support of *Innovate UK* under the *Knowledge Transfer Partnership* scheme is also gratefully acknowledged (Project No. KTP0009933).

7. Data Availability

The raw/processed data required to reproduce these findings cannot be shared at this time due to technical or time limitations.

References

[1] P. K. Rohatgi, N. Gupta, F. Schultz, D. Luong, The synthesis, compressive properties and applications of metal matrix syntactic foams, JOM Journal of the Minerals, Metals & Materials Society 63 (2016) 30–36.

[2] S. E. Zeltmann, B. Chen, N. Gupta, Mechanical properties of epoxy-matrix-borosilicate glass hollow-particle syntactic foams, Materials Performance and Characterization 6 (2017) 11–16.

[3] N. Gupta, S. E. Zeltmann, V. C. Shunmugasamy, D. Pinisetty, Applications of polymer matrix syntactic foams, Journal of Materials 66 (2) (2014) 245–254.

[4] R. Nagorny, N. Gupta, Tensile properties of glass microballoon-epoxy resin syntactic foams, Journal of Applied Polymer Science 102 (2006) 1254–1261.

[5] E. Zegeve, A. K. Ghamsari, E. Woldesenbet, Mechanical properties of graphene platelets reinforced syntactic foams, Composites Part B: Engineering 60 (2015) 268–273.

[6] S. He, D. Carolan, A. Fergusson, A. C. Taylor, Toughening epoxy syntactic foams with milled carbon fibres: Mechanical properties and toughening mechanisms, Materials & Design 169 (2019) 107654.

[7] E. Rizzi, E. Papa, A. Corigliano, Mechanical behaviour of a syntactic foam: experiments and modelling, International Journal of Solids and Structures 37 (2000) 5773–5794.

[8] N. Gupta, E. Woldesenbet, Hygrothermal studies on syntactic foams and compressive strength determination, Composite Structures 61 (2003) 311–320.

[9] N. Gupta, E. Woldesenbet, P. Mensah, Compression properties of syntactic foams: effect of cenosphere radius ratio and specimen aspect ratio, Composites Part A: Applied Science and Manufacturing 35 (2004) 103–111.

[10] L. Wang, J. Zhang, X. Yang, C. Zhang, W. Gong, J. Yu, Flexural properties of epoxy syntactic foams reinforced by fiberglass mesh and/or short glass fibre, Materials & Design 63 (2016) 929–936.

[11] P. Marur, Estimation of effective properties and interface stress concentrations in particulate composites by unit cell methods, Acta Materialia 52 (2004) 1263–1270.

[12] F. V. Antunes, J. A. M. Ferreira, C. Capela, Numerical modelling of the young's modulus of syntactic foams, Finite Elements in Analysis and Design 47 (2011) 78–84.

[13] L. Bardella, A. Sfreddo, C. Ventura, M. Porfiri, N. Gupta, A critical evaluation of micromechanical models for syntactic foams, Mechanics of Materials 50 (2012) 53–69.

[14] M. Yu, P. Zhu, Y. Ma, Experimental study and numerical prediction of tensile strength properties and failure modes of hollow spheres filled syntactic foams, Computational Materials Science 63 (2012) 232–243.

[15] J. Segurado, J. Llorca, A numerical approximation to the elastic properties of sphere-reinforced composites, Journal of the Mechanics and Physics of Solids 50 (2002) 2107–2121.

[16] G. Nian, Y. Shan, Q. Xu, S. Qu, Q. Yang, Failure analysis of syntactic foams: A computational model with cohesive law and XFEM, Composites Part B: Engineering 89 (2004) 18–26.

[17] L. Bardella, G. Perini, A. Panteghini, N. Tessier, N. Gupta, Failure of glass/microballoons/thermoset-matrix syntactic foams subject to hydrostatic loading, European Journal of Mechanics / A Solids 70 (2018) 58–74.

[18] L. Bardella, F. Malance, P. Ponzo, A. Panthegini, M. Porfiri, A micromechanical model for quasi-brittle compressive failure of glass-microballoons/thermoset-matrix syntactic foams, Journal of the European Ceramic Society 34 (2014) 2605–2616.

[19] N. Gupta, R. Ye, M. Porfiri, Comparison of tensile and compressive characteristics of vinyl ester/glass microballoon syntactic foams, Composites: Part B 41 (2010) 236–245.

[20] G. Tagliava, M. Porfiri, N. Gupta, Analysis of flexural properties of hollow-particle filled composites, Composites: Part B 41 (2010) 86–93.

[21] C. Zhang, W. K. Brinienda, R. K. Goldberg, L. W. Kohlmann, Meso-scale modelling of single layer triaxial braided composite using finite element method, Composites Part A: Applied Science and Manufacturing 58 (2014) 36–46.

[22] Q. Meng, Z. Wang, Prediction of interfacial strength and failure mechanisms based on a micromechanical model, Engineering Fracture Mechanics 142 (2015) 170–183.

[23] S. Banerjee, B. Sankar, Mechanical properties of hybrid composites using finite element method based micromechanics, Composites Part B: Engineering 58 (2014) 318–327.

[24] E. Ghossein, M. Levesque, Random generation of periodic hard ellipsoids based on molecular dynamics: A computationally-efficient algorithm, Journal of Computational Physics 253 (2013) 471–490.

[25] B. Widom, Random sequential addition of hard spheres to a volume, The Journal of Chemical Physics 22 (1966) 3888–3894.

[26] R. B. Barello, M. Levesque, Comparison between the relaxation spectra obtained from homogenization models and finite elements for the same composite, International Journal of Solids and Structures 2 (2008) 1279–1298.

[27] B. D. Lubachevsky, F. H. Stillinger, Geometric properties of random disk packings, Journal of Statistical Physics 50 (1990) 561–583.

[28] Abaqus, dassault systemes (2011).

[29] X. H. Chen, Y. W. Mai, Micromechanics of rubber?toughened polymers, Journal of Materials Science 33 (1998) 3529–3539.

[30] K. R. Linger, D. G. Holloway, The fracture energy of glass, Philosophical Magazine 18 (156) (1968) 1269–1280.

[31] 3M microspheres selection guide, multimedia.3m.com/mws/media/1300630/3mtm-glass-bubbles-selection-guide.pdf, accessed: 2017-01-30.

[32] International Standards Organisation, ISO 527-1 Plastics - Determination of Tensile Properties - Part 1: General Principles, Tech. rep., Geneva.

[33] L. E. Nielsen, Simple theory of stress-strain properties of filled polymers, Journal of Applied Polymer Science 10 (1966) 97–103.

[34] L. Nicolais, M. Narkis, Stress-strain behaviour of styrene-acrylonitrile/glass bead composite in the glassy region, Polymer Engineering & Science 11 (1971) 194–199.

[35] D. Carolan, P. Alveen, A. Ivanković, N. Murphy, Effect of notch root radius on fracture toughness of polycrystalline cubic boron nitride, Engineering Fracture Mechanics 78 (2011) 2885–2895.

[36] G. Swaminathan, C. Palanisamy, G. Chidambaram, G. Henri, C. Udyagiri, Enhancing the interfacial strength of glass/epoxy composites using zno nanowires, Composite Interfaces 25 (2018) 151–168.

[37] J. Koyanagi, H. Nakatani, S. Ogihara, Comparison of glass-epoxy interface strengths examined by cruciform specimen and single-fiber pull-out tests under combined stress states., Composites Part A: Applied Science and Manufacturing 43 (2012) 1819–1827.

[38] K. Mai, E. Mader, M. Muhle, Interphase characterisation in composites with new non-destructive methods, Composites Part A: Applied Science and Manufacturing 29 (1998) 1111–1119.

[39] N. Gupta, D. Pinisetty, V. C. Shunmugasamy, Reinforced Polymer Matrix Syntactic Foams: Effect of Nano and Micro-Scale Reinforcement, Springer, 2013.

[40] W. Weibull, A statistical distribution of wide applicability, Journal of Applied Mechanics 18 (1951) 293–297.

[41] K. Trustman, A. D. Jayatilaka, Applicability of Weibull analysis for brittle materials, Journal of Materials Science 18 (1983) 2570–2765.

[42] S. Nohut, C. Lu, Fracture statistics of dental ceramics: discrimination of strength distributions, Ceramics International 38 (2012) 4979–4990.

[43] D. McNamara, D. Carolan, P. Alveen, N. Murphy, A. Ivankovic, The influence of microstructure on the fracture statistics of polycrystalline diamond and polycrystalline cubic boron nitride, Ceramics International 40 (2014) 11543–11549.

[44] J. B. Wachtman, W. R. Cannon, M. J. Matthewson, Mechanical Properties of Ceramics, 2nd Edition, Wiley-Interscience, 1996.

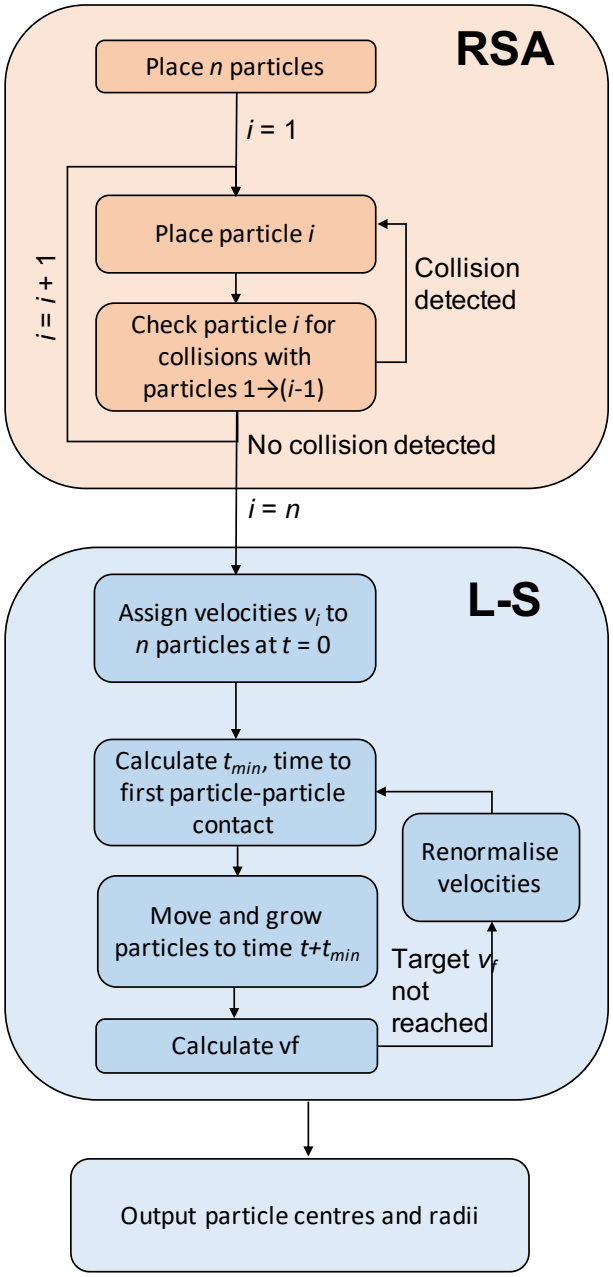

Figure 2: Particle placement algorithm (RSA = Random Sequential Adsorption, L-S = Lubachevsky-Stillinger algorithm).

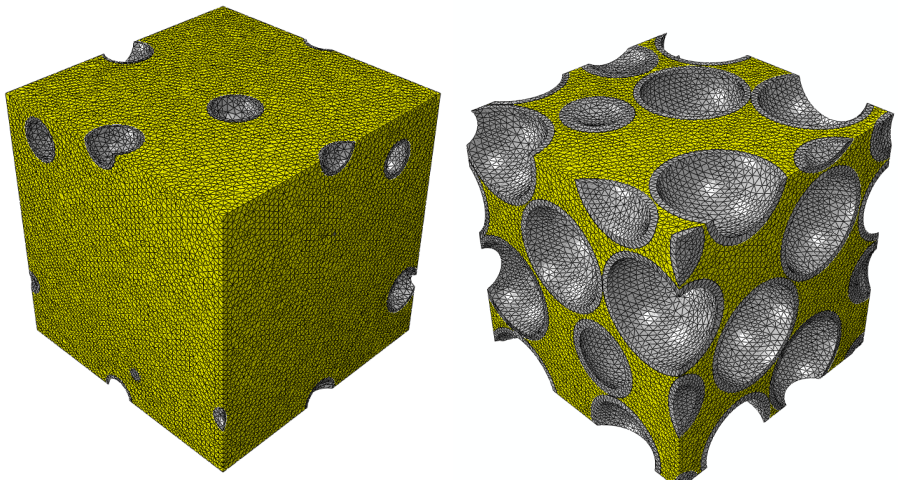

(a) 10 vol.%. (b) 55 vol.%.

Figure 3: The FEA model of the syntactic foam for (a) $v_f = 10\%$ and (b) $v_f = 55\%$. The matrix materials is coloured yellow and the microspheres are shown in grey.

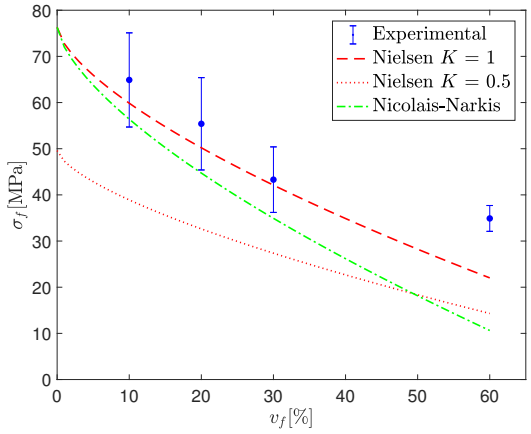

Figure 4: Fracture strength versus microsphere vol.%. Theoretical predictions made using the Nielsen ($K = 1$ and $K = 0.5$) and Nicolais-Narkis models are also shown.

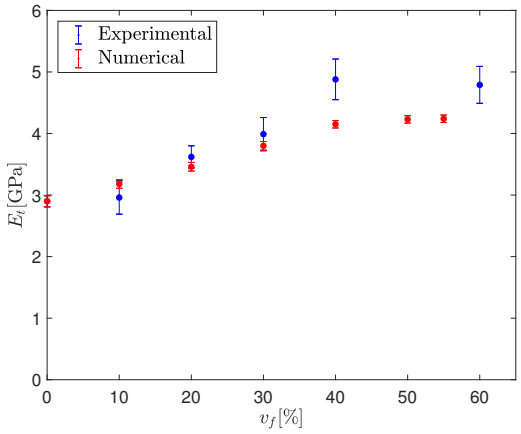

Figure 5: Comparison of experimentally measured Young's modulus with numerical predictions made by the micro-mechanical model.

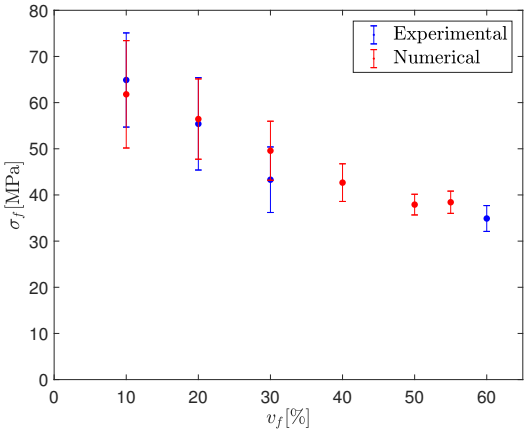

Figure 6: Comparison of experimentally measured failure strength with numerical predictions made by the micro-mechanical model.

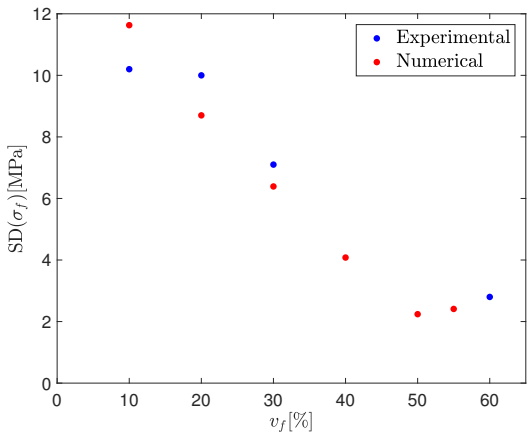

Figure 7: Comparison of the experimentally measured standard deviation of fracture strength with the numerical prediction.

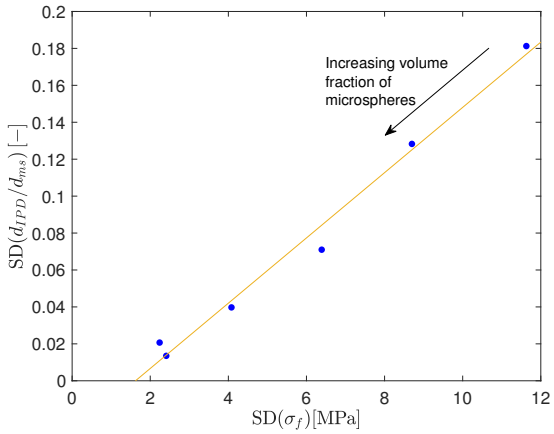

Figure 8: Corrleation between variation in normalised inter-particle distance, d_{IPD}/d_{ms} and syntactic foam tensile fracture strength, σ_f. The linear fit is to guide the reader.

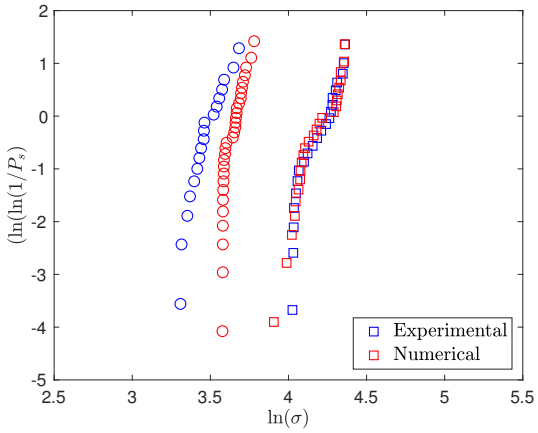

Figure 9: Weibull distribution of experimental measurements and numerical predictions for syntactic foams with 10 vol.% (squares) and 55-60 vol.% (circles).

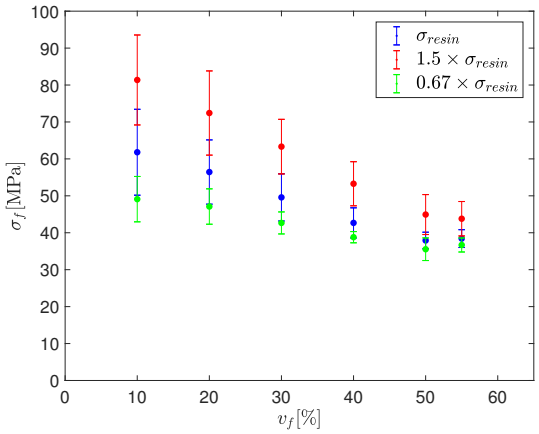

(a) Effect of varying σ_{resin}.

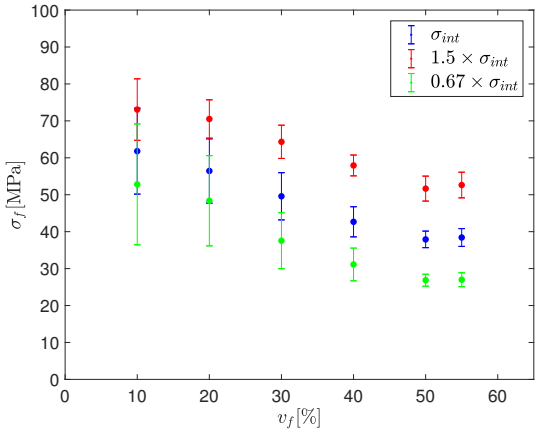

(b) Effect of varying σ_{int}.

Figure 10: Effect of cohesive parameters on the predicted failure strength of composite syntactic foams.

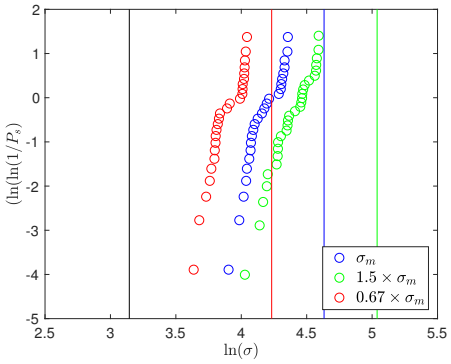

(a) 10 vol.%, effect of varying σ_m.

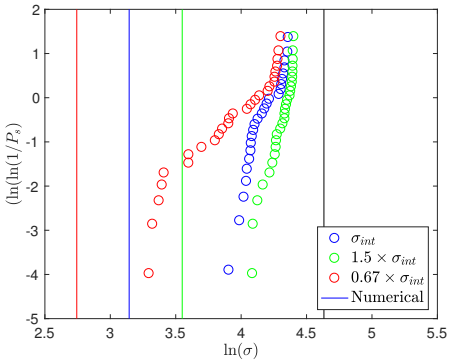

(b) 10 vol.%, effect of varying σ_{int}.

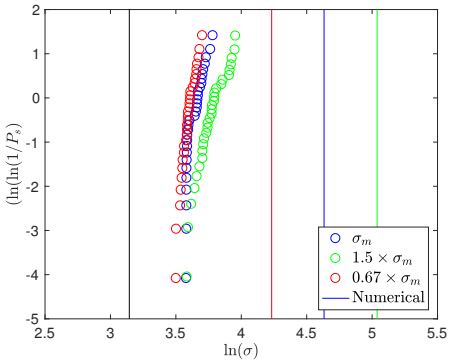

(c) 55 vol.%, effect of varying σ_m.

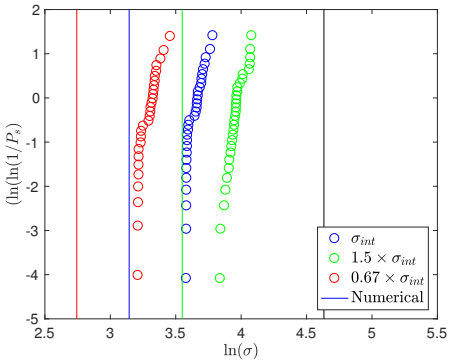

(d) 55 vol.%, effect of varying σ_{int}.

Figure 11: Effect of varying σ_{resin} and σ_{int} on the resultant Weibull distribution.The vertical lines represent the input cohesive strength values for σ_m and σ_{int}.